Journal Pre-proofs

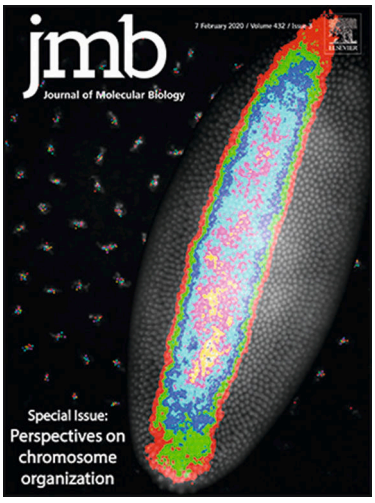

Communication

The Cryo-EM structure of renal amyloid fibril suggests structurally homogeneous multiorgan aggregation in AL amyloidosis

Sarita Puri, Tim Schulte, Antonio Chaves-Sanjuan, Giulia Mazzini, Serena Caminito, Carlo Pappone, Luigi Anastasia, Paolo Milani, Giampaolo Merlini, Martino Bolognesi, Mario Nuvolone, Giovanni Palladini, Stefano Ricagno

PII: S0022-2836(23)00314-5
DOI: https://doi.org/10.1016/j.jmb.2023.168215
Reference: YJMBI 168215

To appear in: *Journal of Molecular Biology*

Received Date: 11 June 2023
Revised Date: 15 July 2023
Accepted Date: 24 July 2023

Please cite this article as: S. Puri, T. Schulte, A. Chaves-Sanjuan, G. Mazzini, S. Caminito, C. Pappone, L. Anastasia, P. Milani, G. Merlini, M. Bolognesi, M. Nuvolone, G. Palladini, S. Ricagno, The Cryo-EM structure of renal amyloid fibril suggests structurally homogeneous multiorgan aggregation in AL amyloidosis, *Journal of Molecular Biology* (2023), doi: https://doi.org/10.1016/j.jmb.2023.168215

The Cryo-EM structure of renal amyloid fibril suggests structurally homogeneous multiorgan aggregation in AL amyloidosis

Sarita Puri[1], Tim Schulte[2], Antonio Chaves-Sanjuan[1,3], Giulia Mazzini[4,5], Serena Caminito[4,5], Carlo Pappone[2,6,7], Luigi Anastasia[2,6], Paolo Milani[4,5], Giampaolo Merlini[4,5], Martino Bolognesi[1,3], Mario Nuvolone[4,5], Giovanni Palladini[4,5], Stefano Ricagno[1,2*]

1. Department of Biosciences, Università degli Studi di Milano, Milan, Italy.
2. Institute of Molecular and Translational Cardiology, IRCCS Policlinico San Donato, 20097, Milan, Italy.
3. Pediatric Research Center Fondazione R.E. Invernizzi and NOLIMITS Center, Università degli Studi di Milano, Milan, Italy.
4. Department of Molecular Medicine, University of Pavia, Pavia, Italy.
5. Amyloidosis Research and Treatment Center, Fondazione IRCCS Policlinico San Matteo, Pavia, Italy.
6. Faculty of Medicine, University of Vita-Salute San Raffaele, 20132 Milan, Italy.
7. Arrhythmia and Electrophysiology Department, IRCCS Policlinico San Donato, San Donato, 20097 Milan, Italy.

***** To whom correspondence may be addressed: E-mail address: Stefano.ricagno@unimi.it

Abstract

Immunoglobulin light chain amyloidosis (AL) is caused by the aberrant production of amyloidogenic light chains (LC) that accumulate as amyloid deposits in vital organs. Distinct LC sequences in each patient yield distinct amyloid structures. However different tissue microenvironments may also cause identical protein precursors to adopt distinct amyloid structures. To address the impact of the tissue environment on structural polymorphism of amyloids, we extracted fibrils from the kidney of an AL patient (AL55) whose cardiac amyloid structure was previously determined by our group. Here we show that the 4.0 Å resolution cryo-EM structure of the renal fibril is virtually identical to that reported for the cardiac fibril. These results provide the first

structural evidence that LC amyloids independently deposited in different organs of the same AL patient share a common fold.

Keywords

Light chains; amyloid-fibril structure; cryo-electron microscopy; AL amyloidosis; multiorgan fibril deposition.

Introduction

Amyloidosis is a group of severe and progressive diseases in which amyloid fibrils deposit in tissues and organs throughout the body [1]. In general, amyloidosis may be localized or systemic [2]. Among systemic amyloidoses, AL amyloidosis is caused by a rare plasma cell dyscrasia with an annual incidence of about ten new cases per million people, representing the most common systemic amyloid disease in high-income countries [3]. A proliferating plasma cell clone overexpresses an amyloidogenic LC that misfolds and forms amyloids. Accumulation of these amyloids alters tissue architecture and ultimately causes fatal organ dysfunction [3]. Each AL patient bears a unique amyloidogenic LC sequence due to genomic recombination and somatic mutations [4, 5, 6]. Indeed, all structures of AL amyloid belonging to different LC germlines λ1 (PDB: 7NSL, 6IC3), λ3 (PDB: 6Z1O, 6Z1I), and λ6 (PDB: 6HUD) extracted from different AL patients differ in both sequences and arrangement of β-strands in their respective 3D structures (Supporting Figure S1) [7, 8, 9, 10].

AL amyloidosis is also a heterogeneous disease in terms of organ involvement. It affects the heart in approximately 75% of total cases, followed by kidneys (65%). Virtually any organ except the central nervous system can be affected. In most cases, multiple organs are affected concurrently [3]. Notable, aggregated LCs have not been detected in blood circulation and it is widely accepted that LC amyloidogenic precursors deposit independently in different organs [11, 12]. When amyloidogenic precursors reach sufficiently high local concentrations, fibril nucleation and growth outcompete degradation mechanisms [2, 13]. The binding of the amyloidogenic precursors with cell surface receptors or components of the extracellular matrix, including proteoglycans, glycosaminoglycans, and collagen fibrils, may favor local accumulation, providing a scaffold for fibril growth and preventing amyloid degradation [14, 15, 16, 17, 18, 19]. A high degree of variation across different tissues and organs exists in terms of cell surface proteins/receptors (the so-called “surfaceome”) [20] extracellular matrix components and adhesion complexes (the “matrisome” and “adhesome”) [21, 22]. Different tissues and organs differ substantially in overall architecture and 3D topology of the extracellular space, interstitial fluid composition, proteolytic activities, and fluid shear forces [23] which could impact amyloidogenesis [2, 24, 25, 26, 27, 28, 29]. In particular, the presence of specific proteases in distinct tissues may affect the stability of full-length LCs differently and in some cases unleash proteolyzed amyloidogenic fragments [29]. Thus, anatomical, biochemical, and biophysical differences across different body sites may modulate the dynamics and

magnitude of amyloid fibril formation, remodeling, and degradation, thus playing a central role in defining amyloid organ tropism. In particular, *IGLV6-57* (λ6) is one of the most overrepresented germlines in AL patients and it is typically associated with renal involvement [30].

However, it is unclear how the tissue microenvironment affects the amyloid structure of sequence-identical LCs in multiple organs of AL patients. Is it the LC sequence or the extracellular environment that defines amyloid structure? The answer to this question could help to develop molecules capable of dissolving preformed amyloid deposits. Whether potential anti-aggregants need to be patient-specific or patient- and organ-specific is instrumental for rational drug design.

So far, low-resolution analysis of fibrils extracted from three tissues of two AL patients revealed comparable morphologies and biophysical properties [31]. However, higher resolution data are required to define whether amyloids share the same fibrillar fold or are polymorphic. All these considerations prompted us to determine the cryo-EM structure of amyloid fibrils extracted from the kidney (renal AL55) of an AL patient designated as AL55 and to compare it with the already reported cardiac AL55 amyloid fibril structure [10]. Our comparative study reveals almost identical folds, suggesting that the LC sequence takes precedence over the organ microenvironment to define its amyloid structure.

Results

The AL55 patient, whose cardiac fibrils have been previously reported, also showed significant proteinuria (15.9 g/24h) and stage II kidney damage due to fibril deposition [10]. Thus, amyloid fibrils were extracted from the renal tissue to compare their structure with that of the cardiac amyloid from the same patient. Cryo-EM micrographs of vitrified amyloids revealed a homogenous population of straight fibrils with an estimated cross-over length and width of 530 ± 50 Å and 104 ± 25 Å, respectively (Figure 1A, Supporting Figure S2A). 2D class averages revealed a well-defined core surrounded by a disordered region (Figure 1B, Supporting Figure S2B). The final 3D map was reconstructed with a helical twist and rise parameters of -1.63° and 4.9 Å, respectively, to a nominal resolution of ~4.0 Å, as estimated from Fourier shell correlations ($FSC_{0.143}$) (Supporting Figure S2E, S2F). The spatial resolution of 4.0 Å is sufficient to establish the overall fibril topology and fold. The local resolution of the fibril cross-section varies from a high-resolution core at the fibril center surrounded by low-resolution edges for which a structural model could not be built (Figures 1C, 1D, and Supporting Figure S3). The dimensions and reconstruction parameters of the fibril essentially match those we reported previously for the AL55 cardiac amyloid structure [10]. Similar to the cardiac fibril model, the model building of the renal fibril indicates that the core region is divided into two peptide segments: (i) a snail-shaped inner core formed by residues Asn-1 to Tyr-37, and (ii) a C-shaped arm formed by residues Ser-66 to Gly-105. The two parts are covalently linked through the Cys-22: Cys-91 disulfide bond (Figure 1E). Each chain comprises nine consecutive β-strands. The Asn-1 to Tyr-37 segment comprises strands from β1 to β5 while the residues Ser-66 to Gly-105 are organized into four strands from β6 to β9 (Figure 1F).

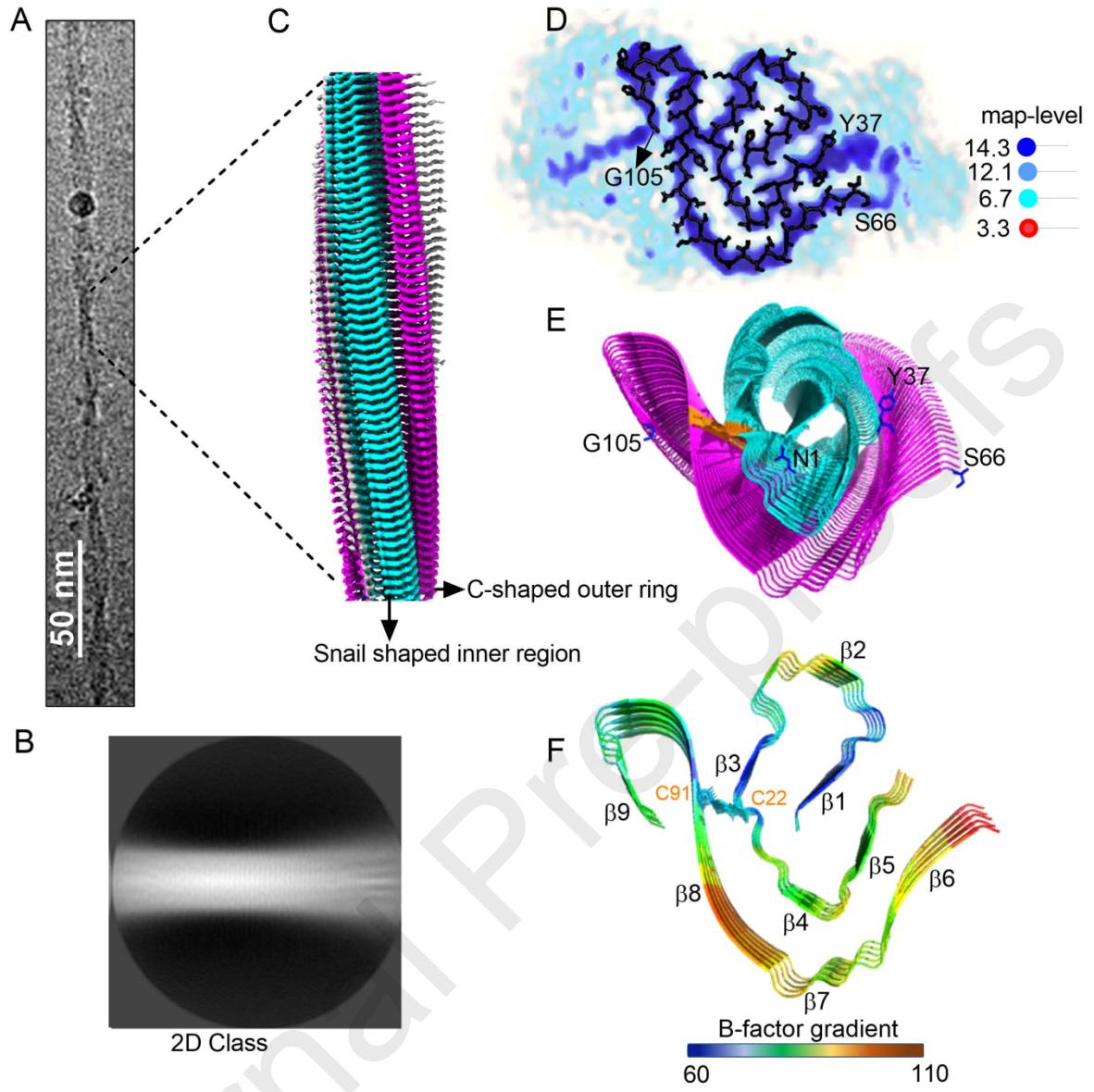

Figure 1. CryoEM reconstruction of renal AL55 amyloid fibril. (A) Representative cryoEM image of a single straight fibril (scale bar 50 nm). (B) Representative 2D class average. (C) Side-view of the reconstructed 3D map (256 nm). N-terminal (snail-shaped) and C-terminal (C-shaped) densities are colored in cyan and magenta, respectively. The unstructured region is shown in grey. (D) A cross-section view of the reconstructed 3D map with the superimposed molecular model. (E) Top view of the molecular model. The color coding for N-terminal residues (Asn-1 to Tyr-37) and C-terminal residues (Ser-66 to Gly-105) are the same as a map in Figure C. The disulfide bond joining two regions is shown in orange color. (F) Five stacks (subunits) in a cross-β arrangement colored according to the overall B-factor values.

A model-based superimposition of the two maps highlights their almost identical morphologies (Figures 2A and 2B). However, we noticed a larger deviation of the C-terminal region caused by a 1-2 Å translational shift along the fibril axis (Figure 2B (third panel) and 2C). In contrast to the cardiac map, the renal map reveals clear features to position the disulfide bond (Figure 2A). The model was adjusted

accordingly leading to a translational shift of residues following Cys-91. Therefore, the Cα-positions of residues Asn-1 to Tyr-94 and Asp-95 to Gly-105 deviate from each other with rmsd values of 0.7 and 3 Å, respectively (Figures 2C and Supporting Figure S4A). The overall juxtaposition of β-sheets in the renal fibril model is fully comparable with the cardiac fibril structure, with a slight difference in the C-shaped region (Supporting Figure S4B). Common to many amyloid structures [32], the monomeric subunits of AL55 amyloid fibrils (renal and cardiac) are not planar relative to the fibril elongation z-axis. While the C-shaped region is mostly planar, the snail-shaped region shows a rise spanning three fibrillar layers from residue Asn1 to Tyr37, as observed in the cardiac fibril (Supporting Figure S4C). Analogies between the renal and cardiac amyloids also extend beyond the fibril core to the low-resolution edges between residues Glu-38 to Gly-65 and after Gly-105 (Figure 2A). In both cases, low-resolution regions suggest that the segment Glu-38 to Gly-65 and residues following Gly-105 are flexible. Sequentially, these stretches are rich in Gly, Pro, and charged residues which are not compatible to form β-sheet structures (Supporting Figure S4D). Moreover, the solubilized fibrils contain a significant amount of full-length LCs and intact variable domain [32] indicating that proteolysis is unlikely to cause these regions to be invisible in the fibril reconstruction. The data here presented collectively establish the homogenous multi-organ aggregation of the AL55 light chain to form virtually identical fibrillar structures, despite their independent growth in distinct micro-environments.

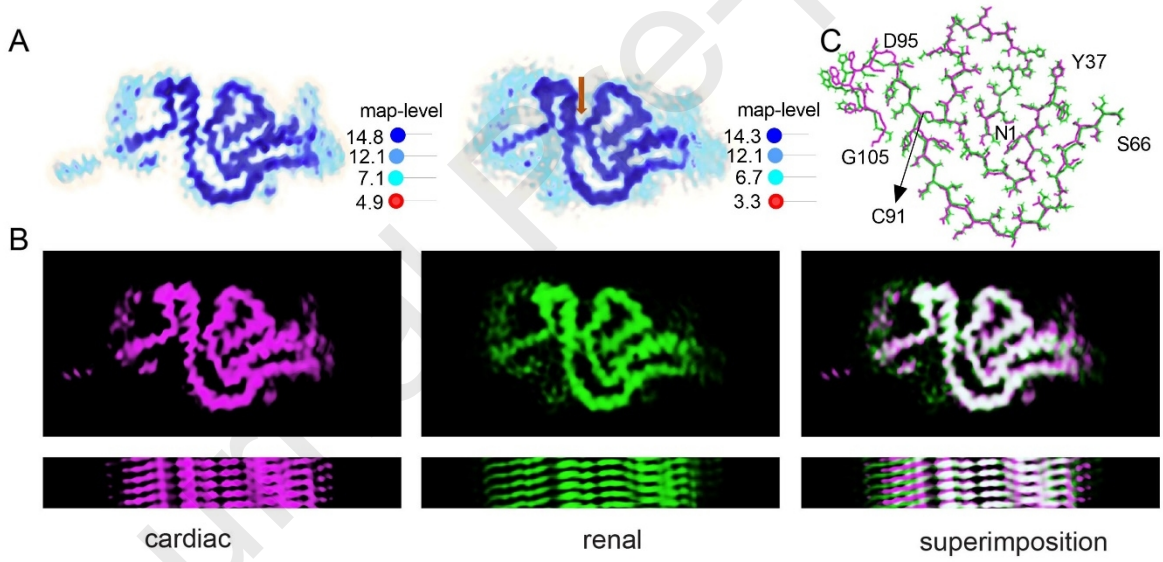

Figure 2. Map-model comparison between renal and cardiac fibrils. (A) cardiac and renal maps with corresponding contour levels. The Coulomb potential corresponding to the disulfide bond is highlighted in the renal map with an orange arrow. (B) Cross-sectional and side-views of superimposed maps. (C) Superimposed models. The complete amino-acid sequence of the variable domain contributed to the fibril core is shown in Supporting Figure S4D.

Discussion

The steadily expanding database of amyloid structures has revealed that amyloids do not follow the “one sequence – one fold” dogma of globular domains (Amyloid Atlas) [33]. However, Shi and co-workers suggested a “one disease – one fold” framework based on the observation that tau fibrils extracted from patients with the same disease share the same amyloid fold [34]. Notably, despite the high sequence conservation of

serum amyloid A (SAA) in different mammals, *ex-vivo* structures from different species display independent amyloid folds [35, 36, 37]. Moreover, human AA amyloid deposited in two independent renal compartments (glomeruli and medulla), adopts different structures, probably due to proteolytic processing [38]. As predicted by the unique nature of each amyloidogenic LC sequence, all four reported structures of cardiac amyloids from AL patients display totally different folds [7, 8, 9, 10].

In this study, we show that the AL55 (Genbank accession code AYV88981), a prototypic LC belonging to *IGLV6-57*, forms amyloid adopting identical amyloid structures in multiple organs of the same patient. Extrapolation of structural information should be taken with caution in the AL field and more Cryo-EM structures of amyloids extracted from different organs of the same AL patient are needed. Nevertheless, our high-resolution structural data and previous reports strongly suggest that the structural identity of the amyloids deposited in different organs may be true for multiple tissues of AL patients. The renal/cardiac structures of AL55 amyloids are fully compatible with the common proteolytic sites present in fibrils extracted from the heart, kidney, and abdominal fat [32, 39]. Furthermore, our cryo-EM structure corroborates the biochemical characterization of AL fibrils from different tissues performed by Annamalai and co-workers [31]. The fibrillar fold shared by fibrils extracted from different organs may indicate a limitation of LC precursors to adopt other structures. Indeed, the conserved disulfide bond in the variable domain of all LC sequences and the presence of Pro residues in specific positions constrain the conformational space available to LC amyloid folds likely resulting in identical fibrillar structures [8, 40]. Moreover, assemblies of *in vivo* amyloid aggregates are likely selected according to their resistance to proteases, further reducing the potential misfolding structural space [41].

In summary, we show that amyloid deposits in two organs of an AL patient assemble into a virtually identical cross-β fold. Based on the present results and the above considerations we propose that the sequence of amyloidogenic LCs and not the extracellular environment - determines amyloid assembly *in vivo*. These results imply that potential anti-amyloid treatments are expected to have a systemic multi-organ effect in AL patients.

Materials and Methods

Fibril extraction, cryo-EM sample preparation, and data collection

A standard fibril extraction protocol optimized by Swuec and coworkers [10] was used to extract renal AL55 amyloid fibrils. Briefly, about 500 mg of kidney tissue was washed in Tris calcium buffer (20 mM Tris, 140 mM NaCl, 2 mM $CaCl_2$, pH 8.0) multiple times followed by overnight treatment with *Clostridium histolyticum* collagenase at a final concentration of 5 mg/ml at 37°C. After treatment, the collected pellet was washed 10 times with Tris EDTA buffer (20 mM Tris, 140 mM NaCl, 10 mM EDTA, pH 8.0). The final pellet obtained after this step was resuspended in 400 µl of ice-cold deionized water. The homogenate was centrifuged for 5 min at 3100 *g* at 4 °C and the supernatant was collected for cryo-EM grid preparation. A 4-µl sample containing extracted fibrils was applied onto a glow-discharged C-Flat thick 1.2/1.3 Cu 300-mesh grid. The sample was immediately blotted and then rapidly plunge-frozen into liquid ethane without incubation on the grid. The vitrification of the sample was carried out using a Mark IV Vitrobot (Thermo Fisher Scientific, U.S.A.). The vitrified grids were

then transferred to a Talos Arctica (Thermo Fisher Scientific, U.S.A.) operating at 200 kV and equipped with a Falcon 3 direct electron detector (Thermo Fisher Scientific, U.S.A.). A total of 1,800 movies were acquired using EPU 2.8 (Thermo Fisher Scientific, U.S.A.) in electron counting mode with an applied dose of 40 e-/Å^2, which was divided into 40 frames at a magnification of 120k, corresponding to a pixel size of 0.889 Å/pixel, and a defocus range of -0.8 to -2.6 µm.

Helical reconstruction

Multi-frame movies were dose-weighted, motion- and CTF-corrected by MotionCor2 [42] and CTFFIND4.1 [43] in RELION 3.1 [44, 45, 46]. 9452 fibrils were manually picked from 1431 selected micrographs. A first set of 28,069 segments was extracted in 768-pixel boxes with a 10% inter-box distance. Tube diameter, rise, and number of asymmetric units (NSU) were set to 150 Å, 4.75 Å, and 18, respectively. A single large class average was selected from reference-free 2D classes to generate an initial model with an estimated crossover distance of 550 Å. A second set of 91,877 smaller segments was extracted with a box size of 320 pixels and 10% inter-box distance. The helical tube diameter, rise, and asymmetrical unit values were set to 140 Å, 4.75 Å, and 6, respectively. An initial and following set of reference-free 2D classes were obtained with T-regularization values of 2 and 4, respectively. The initial model was low pass filtered to 60 Å for reference-based 3D classification with a T-regularization value of 4. A single 3D class was low pass filtered to 30 Å and used to perform the first round of 3D classification with four classes and a T-regularization value of 10. Three good-looking classes were selected for another round of 3D classification with a T-regularization value of 10. Another round of 3D classification with four classes was carried out on selected 69602 segments from the previous round. Three high-resolution classes were selected for 3D auto-refinement. A total of 49091 segments were used for the final 3D auto-refinement using a 5 Å low-pass filtered reference map, a helical-z parameter of 30%, and a tau-fudge value of 20. The two half maps obtained from the 3D auto-refinement were aligned together and used as a reference model for another round of 3D auto-refinement with C1 symmetry, a helical twist of -1.60°, and a helical rise of 4.9 Å. The refined 3D reconstruction was sharpened using RELION's standard post-processing procedure by applying a soft-edge solvent mask. The overall resolution estimate of the final map was 4.0 Å calculated from FSC at 0.143. The B-factor value for the post-processed 3D map was -139, Reconstruction statistics are listed in Supporting Table S1.

Model building and refinement

The cardiac AL55 amyloid fibril structure fit into the post-processed 3D map of the renal AL55 amyloid fibril in UCSF-Chimera and was used as a reference model for model building [47]. Using reference model restraints, the model was refined iteratively in UCSF-ChimeraX/Isolde, COOT, and PHENIX [47, 48 49, 50]. Molprobity was used to validate model statistics [51]. Final model statistics are listed in Supporting Table S1.

Structural data presentation

The reconstructed map and refined model images were created using UCSF-chimeraX [47] and PyMoL. Rmsd values were calculated using PyMoL.

Accession numbers

Cryo-EM raw data, 3D map, and final structure of renal AL55 fibrils have been deposited with accession codes EMPIAR-11446, EMD-16780, and 8CPE at EMPIAR, EMDB, and RCSB data banks, respectively. The referenced cardiac AL55 fibril 3D map and model information are publicly available under accession codes EMD-0274 and 6HUD, respectively [10].

Acknowledgments

This work was supported by the Italian Ministry of Research PRIN 2020 (20207XLJB2) (G.P., S.R.), Ricerca Corrente funding from the Italian Ministry of Health to IRCCS Policlinico San Donato (S.R.), Italian Ministry of Health (Ricerca Finalizzata, grant #GR-2018-12368387) (M.N.), CARIPLO Foundation (grant #2018-0257) (M.N.), Cancer Research UK [C355/A26819], FC AECC and AIRC under the Accelerator Award Program (G.Mer., G.P., M.N.). We kindly acknowledge the University of Milan Unitech NOLIMITS Center for granting access to the cryo-EM facility.

CRediT authorship contribution statement

Sarita Puri: Investigation, analysis, data visualization, original draft written and edited; **Tim Schulte, Antonio Chaves-Sanjuan**: Data analysis, Data edited and reviewed, manuscript edited**; Giulia Mazzini**: Fibril extraction, manuscript edited. **Giampaolo Merlini, Giovanni Palladini, Mario Nuvolone**: Funding and resources acquisition; **Martino Bolognesi**: Manuscript edited; **Stefano Ricagno**: Conceptualization, Supervision, Funding acquisition, Manuscript edited and reviewed, funding and resources acquisition. Contribution to and approval of the submitted version by all authors.

Competing interests

The authors declare no conflict of interest.

References

1. Wechalekar, A. D., Gillmore, J. D., Hawkins, P. N. (2016). Systemic amyloidosis. *The Lancet*. **387**, 2641–2654.
2. Merlini, G., Bellotti, V. (2003). Molecular mechanisms of amyloidosis. *N. Engl. J. Med*. **349**, 583–596.
3. Merlini, G., Dispenzieri, A., Sanchorawala, V., Schönland, S. O., Palladini, G., Hawkins, P. N., Gertz, M. A. (2018). Systemic immunoglobulin light chain amyloidosis, *Nat. Rev. Dis. Primers*. **4**, 38.
4. Blancas-Mejia, L. M., Misra, P., Dick, C. J., Cooper, S. A., Redhage, K. R., Bergman, M. R., Jordan, T. L., Maar, K., Ramirez-Alvarado, M. (2018). Immunoglobulin light chain amyloid aggregation. *Chem. Commun*. **54**, 10664–10674.

5. Cascino, P., Nevone, A., Piscitelli, M., Scopelliti, C., Girelli, M., Mazzini, G., Caminito, S., Russo, G., Milani, P., Basset, M., Foli, A., Fazio, F., Casarini, S., M. Massa, M. Bozzola, J. Ripepi, M.A. Sesta, G. Acquafredda, M. De Cicco, Moretta, A., Rognoni, P., Milan, E., Ricagno, S., Lavatelli, F., Petrucci, M. T., Miho, E., Klersy, C., Merlini, G., Palladini, G., M. Nuvolone, M. (2022). Single-molecule real-time sequencing of the M protein: Toward personalized medicine in monoclonal gammopathies. *American J. Hematol*. **97**, E389-E392.
6. Poshusta, T. L., Sikkink, L. A., Leung, n., Clark, R. J., Dispenzieri, A., Ramirez-Alvarado, M. (2009). Mutations in specific structural regions of immunoglobulin light chains are associated with free light chain levels in patients with AL Amyloidosis. *PLoS ONE*. **4**, e5169.
7. Radamaker, L., Baur, J., Huhn, S., Haupt, C., Hegenbart, U., Schönland, S., Bansal, A., Schmidt, M., Fändrich, M. (2021). Cryo-EM reveals structural breaks in a patient-derived amyloid fibril from systemic AL amyloidosis, *Nat. Commun*. **12**, 875.
8. Radamaker, L., Karimi-Farsijani, S., Andreotti, G., Baur, J., Neumann, M., Schreiner, S., Berghaus, N., Motika, R., Haupt, C., Walther, P., Schmidt, V., Huhn, S., Hegenbart, U., Schönland, S.O., Wiese, S., Read, C., Schmidt, M., Fändrich, M. (2021). Role of mutations and post-translational modifications in systemic AL amyloidosis studied by cryo-EM. *Nat. Commun.* **12**, 6434.
9. Radamaker, L., Lin, Y.-H., Annamalai, K., Huhn, S., Hegenbart, U., Schönland, S.O., Fritz, G., Schmidt, M., Fändrich, M. (2019). Cryo-EM structure of a light chain-derived amyloid fibril from a patient with systemic AL amyloidosis. *Nat. Commun.* **10**, 1103.
10. Swuec, P., Lavatelli, F., Tasaki, M., Paissoni, C., Rognoni, P., Maritan, M., Brambilla, F., Milani, P., Mauri, P., Camilloni, C., Palladini G., Merlini, G., Ricagno, S., Bolognesi, M. (2019). Cryo-EM structure of cardiac amyloid fibrils from an immunoglobulin light chain AL amyloidosis patient. *Nat. Commun*. **10**,1269.
11. Lavatelli, F. (2022). Mechanisms of organ damage and novel treatment targets in AL Amyloidosis. *Hemato*. **3**, 47–62.
12. Palladini, G., Lavatelli, F., Russo, P., Perlini, S., Perfetti, V., Bosoni, T., Obici, L., Bradwell, A. R., D'Eril, G. M., Fogari, R., Moratti, R., Merlini, G. (2006). Circulating amyloidogenic free light chains and serum N-terminal natriuretic peptide type B decrease simultaneously in association with improvement of survival in AL. *Blood*. **107**, 3854–3858.
13. Jarrett, J. T., Lansbury, P. T. (1993). Seeding "one-dimensional crystallization" of amyloid: A pathogenic mechanism in Alzheimer's disease and scrapie? *Cell.* **73**, 1055–1058.
14. Yan, S. D., Zhu, H., Zhu, A., Golabek, A., Du, H., Roher, A., Yu, J., Soto, C., Schmidt, A. M., Stern, D., Kindy, M. (2000). Receptor-dependent cell stress and amyloid accumulation in systemic amyloidosis. *Nat Med*. **6**, 643–651.
15. Teng, J., Russell, W. J., Gu, X., Cardelli, J., Jones, M. L., Herrera, G. A. (2004). Different types of glomerulopathic light chains interact with mesangial cells using a common receptor but exhibit different intracellular trafficking patterns. *Lab. Invest*. **84**, 440–451.
16. Herrera, G. A., Del Pozo-Yauner, L., Teng, J., Zeng, C., Shen, X., Moriyama, T., Ramirez Alcantara, V., Liu, B., Turbat-Herrera, E. A. (2021). Glomerulopathic light chain-mesangial cell interactions: Sortilin-related receptor (SORL1) and signaling. *Kid. Int. Rep*. **6**,1379–1396.

17. Stevens, F. J., Kisilevsky, R. (2000). Immunoglobulin light chains, glycosaminoglycans, and amyloid. *Cell. Mol. Life Sci.* **57**, 441–449.
18. Harris, D. L., King, E., Ramsland, P. A., Edmundson, A. B. (2000). Binding of nascent collagen by amyloidogenic light chains and amyloid fibrillogenesis in monolayers of human fibrocytes. *J. Mol. Recognit.* **13**, 198–212.
19. Jackson, J. W., Foster, J. S., Martin, E. B., Macy, S., Wooliver, C., Balachandran, M., Richey, T., Heidel, R. E., Williams, A. D., Kennel, S. J., Wall, J. S. (2022). Collagen inhibits phagocytosis of amyloid *in-vitro* and *in-vivo* and may act as a 'don't eat me' signal. *Amyloid*. 1–12.
20. Bausch-Fluck, D., Hofmann, A., Bock, T., Frei, A. P., Cerciello, F., Jacobs, A., Moest, H., Omasits, U., Gundry, R. L., Yoon, C., Schiess, R., Schmidt, A., Mirkowska, P., Härtlová, A., Van Eyk, J. E., Bourquin, J.-P., Aebersold, R., Boheler, K. R., Zandstra, P., Wollscheid, B. (2015). A mass spectrometric-derived cell surface protein atlas. *PLoS ONE*. **10**, e0121314.
21. McCabe, M. C., Saviola, A. J., Hansen, K. C. (2023). Mass spectrometry-based atlas of extracellular matrix proteins across 25 mouse organs. *J. Proteome Res*. **22**, 790–801.
22. Krasny, L., Huang, P. H. (2021). Advances in the proteomic profiling of the matrisome and adhesome. *Exp. Rev. of Prot.* **18**, 781–794.
23. Park, S., Jung, W.-H., Pittman, M., Chen, J., Chen, Y. (2020). The effects of stiffness, fluid viscosity, and geometry of microenvironment in homeostasis, aging, and diseases: A brief review. *J. Biomechan. Eng*. **142**, 100804.
24. Stix, B., Kähne, T., Sletten, K., Raynes, J., Roessner, A., Röcken, C. (2001). Proteolysis of AA amyloid fibril proteins by matrix metalloproteinases 1, -2, and -3. *American J. Path*. **159**, 561–570.
25. Chen, C.-D. (2001). Furin initiates gelsolin familial amyloidosis in the Golgi through a defect in Ca2+ stabilization. *EMBO J*. **20**, 6277–6287.
26. Kim, S.-H., Wang, R., Gordon, D. J., Bass, J., Steiner, D. F., Lynn, D. G., Thinakaran, G., Meredith, S. C., Sisodia, S. S. (1999). Furin mediates enhanced production of fibrillogenic Aβ peptides in familial British dementia. *Nat Neurosci.* **2**, 984–988.
27. Hill, E. K., Krebs, B., Goodall, D. G., Howlett, G. J., Dunstan, D. E. (2006). Shear flow induces amyloid fibril formation. *Biomacromolecules*. **7**, 10–13.
28. Marcoux, J., Mangione, P. P., Porcari, R., Degiacomi, M. T., Verona, G., Taylor, G. W., Giorgetti, S., Raimondi, S., Sanglier-Cianférani, S., Benesch, J. L., Cecconi, C., Naqvi, M. M., Gillmore, J. D., Hawkins, P. N., Stoppini, M., Robinson, C. V., Pepys, M. B., Bellotti, V. (2015). A novel mechano-enzymatic cleavage mechanism underlies transthyretin amyloidogenesis. *EMBO Mol Med*. **7**, 1337–1349.
29. Enqvist, S., Sletten, K., Westermark, P. (2009). Fibril protein fragmentation pattern in systemic AL-amyloidosis: Fragmentation pattern in AL-amyloidosis. *J. Pathol*. **219**, 473–480.
30. Del Pozo-Yauner, L., Turbat-Herrera, E. A., Pérez-Carreón, J. I., Herrera, G. A. (2022). From the light chain sequence to the tissue microenvironment: contribution of the mesangial cells to glomerular amyloidosis. *Hemato*. **3**, 232–267.
31. Annamalai, K., Liberta, F., Vielberg, M.-T., Close, W., Lilie, H., Gührs, K.-H., Schierhorn, A., Koehler, R., Schmidt, A., Haupt, C., Hegenbart, U., Schönland, S., Schmidt, M., Groll, M., Fändrich, M. (2017). Common fibril structures imply

systemically conserved protein misfolding pathways *in-vivo*. *Angew. Chem. Int. Ed.* **56**, 7510–7514.
32. Mazzini, G., Ricagno, S., Caminito, S., Rognoni, P., Milani, P., Nuvolone, M., Basset, M., Foli, A., Russo, R., Merlini, G., Palladini, G., Lavatelli, F. (2022). Protease-sensitive regions in amyloid light chains: what a common pattern of fragmentation across organs suggests about aggregation. *FEBS J*. **289**, 494–506.
33. Sawaya, M. R., Hughes, M. P., Rodriguez, J. A., Riek, R., Eisenberg, D. S. (2021). The expanding amyloid family: Structure, stability, function, and pathogenesis. *Cell*. **184**, 4857–4873.
34. Shi, Y., Zhang, W., Yang, Y., Murzin, A. G., Falcon, B., Kotecha, A., Van Beers, M., Tarutani, A., Kametani, F., Garringer, H. J., Vidal, R., Hallinan, G. I., Lashley, T., Saito, Y., Murayama, S., Yoshida, M., Tanaka, H., Kakita, A., Ikeuchi, T., Robinson, A. C., Mann, D. M. A., Kovacs, G. G., Revesz, T., Ghetti, B., Hasegawa, M., Goedert, M., Scheres, S. H. W. (2021). Structure-based classification of tauopathies. *Nature*. **598**, 359–363.
35. Liberta, F., Loerch, S., Rennegarbe, M., Schierhorn, A., Westermark, P., Westermark, G.T., Hazenberg, B. P. C., Grigorieff, N., Fändrich, M., Schmidt, M. (2019). Cryo-EM fibril structures from systemic AA amyloidosis reveal the species complementarity of pathological amyloids. *Nat. Commun*. **10**, 1104.
36. Bansal, A., Schmidt, M., Rennegarbe, M., Haupt, C., Liberta, F., Stecher, S., Puscalau-Girtu, I., Biedermann, A., Fändrich, M. (2021). AA amyloid fibrils from diseased tissue are structurally different from *in-vitro* formed SAA fibrils. *Nat. Commun*. **12**, 1013.
37. Schulte, T., Chaves-Sanjuan, A., Mazzini, G., Speranzini, V., Lavatelli, F., Ferri, F., Palizzotto, C., Mazza, M., Milani, P., Nuvolone, M., Vogt, A.-C., Vogel, M., Palladini, G., Merlini, G., Bolognesi, M., Ferro, S., Zini, E., Ricagno, S. (2022). Cryo-EM structure of *ex-vivo* fibrils associated with extreme AA amyloidosis prevalence in a cat shelter. *Nat. Commun*. **13**, 7041.
38. Banerjee, S., Baur, J., Daniel, C., Pfeiffer, P. B., Hitzenberger, M., Kuhn, L., Wiese, S., Bizjet, J., Haupt, C., Amann, K. U., Zacharias, M., Hazenberg, B. P. C., Westermark, G. T., Schmidt, M., Fändrich, M. (2022) Amyloid fibril structure from the vascular variant of systemic AA amyloidosis. *Nat. Commun*. **13**, 7261.
39. Lavatelli, F., Mazzini, G., Ricagno, S., Iavarone, F., Rognoni, P., Milani, P., Nuvolone, M., Swuec, P., Caminito, S., Tasaki, M., Chaves-Sanjuan, A., Urbani, A., Merlini, G., Palladini, G. (2020). Mass spectrometry characterization of light chain fragmentation sites in cardiac AL amyloidosis: Insights into the timing of proteolysis. *J. Biol. Chem*. **295**,16572–16584.
40. Haupt, C. (2021). The AL amyloid fibril: looking for a link between fibril formation and structure. *Hemato.* **2**, 505–514.
41. Schönfelder, J., Pfeiffer, P. B., Pradhan, T., Bijzet, J., Hazenberg, B. P. C., Schönland, S. O., Hegenbart, U., Reif, B., Haupt, C., Fändrich, M. (2021). Protease resistance of *ex vivo* amyloid fibrils implies the proteolytic selection of disease-associated fibril morphologies. *Amyloid*. **28**, 243–251.
42. Zheng, S. Q., Palovcak, E., Armache, J.-P., Verba, K. A., Cheng, Y., Agard, D. A. (2017). MotionCor2: anisotropic correction of beam-induced motion for improved cryo-electron microscopy. *Nat. Methods*. **14**, 331–332.
43. Rohou, A., Grigorieff, N. (2015). CTFFIND4: Fast and accurate defocus estimation from electron micrographs. *J. Struc. Biol*. **192**, 216–221.
44. Gremer, L., Schölzel, D., Schenk, C., Reinartz, E., Labahn, J., Ravelli, R. B. G., Tusche, M., Lopez-Iglesias, C., Hoyer, W., Heise, H., Willbold, D., Schröder, G.

F. (2017). Fibril structure of amyloid-β (1–42) by cryo–electron microscopy. *Science*. **358**,116–119.
45. He, S., Scheres, S. H. W. (2017). Helical reconstruction in RELION. *J. Struc. Biol.* **198**,163–176.
46. Zivanov, J., Nakane, T., Forsberg, B. O., Kimanius, D., Hagen, W. J., Lindahl, E., Scheres, S. H. (2018). New tools for automated high-resolution cryo-EM structure determination in RELION-3. *eLife*. **7**, e42166.
47. Pettersen, E. F., Goddard, T. D., Huang, C. C., Meng, E. C., Couch, G. S., Croll, T. I., Morris, J. H., Ferrin, T. E. (2021). UCSF CHIMERAX : Structure visualization for researchers, educators, and developers. *Protein Sci*. **30**, 70–82.
48. Croll, T. I. (2018). *ISOLDE*: a physically realistic environment for model building into low-resolution electron-density maps. *Acta Crystallogr. D. Struct. Biol.* **74**, 519–530.
49. Afonine, P. V., Poon, B. K., Read, R. J., Sobolev, O. V., Terwilliger, T. C., Urzhumtsev, A., Adams, P. D. (2018). Real-space refinement in *PHENIX* for cryo-EM and crystallography. *Acta Crystallogr. D. Struct. Biol.* **74**, 531–544.
50. Emsley, P., Cowtan, K. (2004). *Coot*: model-building tools for molecular graphics. *Acta Crystallogr. D. Biol. Crystallogr*. **60**, 2126–2132.
51. Davis, I. W., Leaver-Fay, A., Chen, V. B., Block, J. N., Kapral, G. J., Wang, X., Murray, L. W., Arendall, W. B., Snoeyink, J., Richardson, J. S., Richardson, D. C. (2007). MolProbity: all-atom contacts and structure validation for proteins and nucleic acids. *Nucleic Acids Res*. **35**, W375–W383.

CRediT authorship contribution statement

Sarita Puri: Investigation, analysis, data visualization, original draft written and edited; **Tim Schulte, Antonio Chaves-Sanjuan**: Data analysis, Data edited and reviewed, manuscript edited**; Giulia Mazzini**: Fibril extraction, manuscript edited. **Giampaolo Merlini, Giovanni Palladini, Mario Nuvolone**: Funding and resources acquisition; **Martino Bolognesi**: Manuscript edited; **Stefano Ricagno**: Conceptualization, Supervision, Funding acquisition, Manuscript edited and reviewed, funding and resources acquisition. Contribution to and approval of the submitted version by all authors.

Graphical abstract

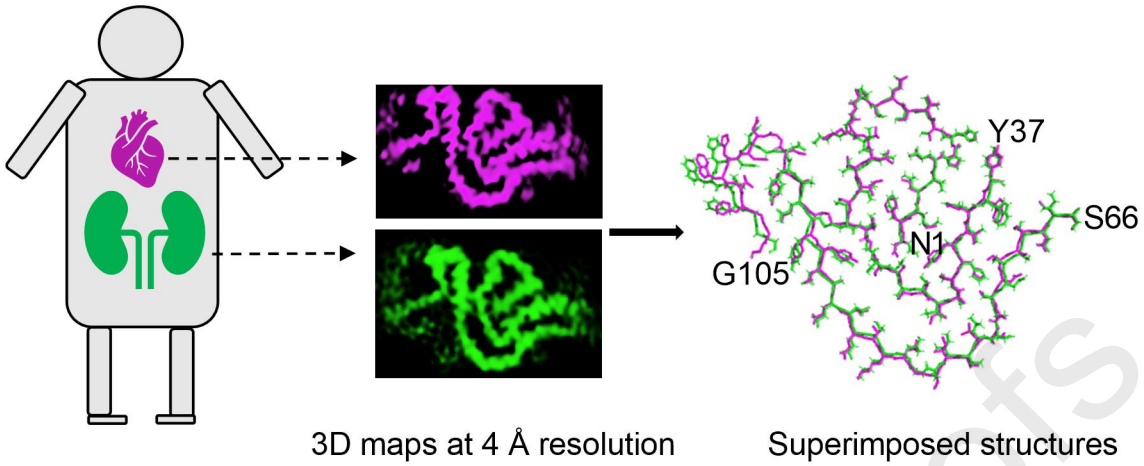

Highlights

1. In AL amyloidosis, light chains independently form amyloids in different organs.
2. 4.0 Å cryo-EM structure of amyloid fibrils from the kidney of an AL patient.
3. Amyloids from kidneys and from heart of the same AL patient share a common fold.
4. AL deposits from different organs of a patient may generally share the same amyloid fold.

Declaration of interests

☒ The authors declare that they have no known competing financial interests or personal relationships that could have appeared to influence the work reported in this paper.

☐The authors declare the following financial interests/personal relationships which may be considered as potential competing interests: